Journal of The Electrochemical Society, **163** (2) H99-H104 (2016)
0013-4651/2016/163(2)/H99/6/$33.00 © The Electrochemical Society

Ethylene Glycol and Ethanol Oxidation on Spinel Ni-Co Oxides in Alkaline

Shengnan Sun,[a] Ye Zhou,[a] Benlin Hu,[a] Qichun Zhang,[a] and Zhichuan J. Xu[a,b,c,z]

[a]*School of Materials Science and Engineering, Nanyang Technological University, Singapore 639798*
[b]*Energy Research Institute, Nanyang Technological University, Singapore 639798*
[c]*Solar Fuel Laboratory, Nanyang Technological University, Singapore 639798*

This article presents a systematic study on the composition dependence of Ni-Co oxides (NCOs) on their electrocatalytic activities toward ethylene glycol (EG) and ethanol (EtOH) oxidation. NCO electrodes were prepared by co-electrodeposition method followed by annealing in air. The atomic ratios of Ni / (Ni + Co) (Ni content) in NCOs were controlled by adjusting the concentration ratio of Ni and Co precursors. As the Ni content increased, the phase of materials changed from the spinel to the mixture of spinel and rock salt. The electrocatalytic activities of these NCOs toward EG and EtOH oxidation were investigated by cyclic voltammetry, differential pulse voltammetry, multi-step chronoamperometry, and electrochemical impedance spectroscopy techniques. It was found that the performance of NCOs for EG and EtOH oxidation exhibited a firstly-increase-then-decrease trend with the increase of Ni content and the best performance was found at 46% Ni. The presence of Ni probably can facilitate EG and EtOH oxidation. Increasing the concentration of reactants or pH can improve the reaction rates. The products from EG and EtOH oxidation were analyzed by nuclear magnetic resonance, which indicated that the oxidation reaction was a process from hydroxyl group to carboxyl group.
 [DOI: 10.1149/2.0761602jes]

Manuscript submitted August 31, 2015; revised manuscript received October 27, 2015. Published November 25, 2015.

Energy and environmental issues have been attracting more and more attention as twin problems in recent years. The current energy infrastructure relying on the fossil fuel is not only threatened by the limited supply, but also generates serious pollution emissions. Great efforts have been made on exploring alternative clean and safe energy resources, such as solar, wind, tide, etc.[1–3] The need of connecting these clean energy resources with smart grids has stimulated great interests on the energy storage and conversion technologies. Ni-Co oxides have attracted great attention in recent years due to their rich redox chemistry, relatively low cost, and high electrochemical activities.[2,4,5] In particular, a large number of investigations have been focused on small molecule oxidation reactions, such as water oxidation reaction,[6,7] urea oxidation,[8] glucose oxidation,[9] and alcohol oxidation.[2,10–12] Ni-Co oxides (e.g. $NiCo_2O_4$) usually exhibit much better electrocatalytic performance than pure Co_3O_4 and NiO, especially for water oxidation. This has been reported by several groups and such better performance has been ascribed to some synergistic effects.[2,8,13] For example, the earlier investigation showed that Ni-Co oxides with ~32% Ni gave the highest activity in water oxidation reaction due to the higher conductivity of $NiCo_2O_4$.[6,14] The recent study reported that giving more Ni may improve the water oxidation activity due to the structure transformation.[7] $NiCo_2O_4$ and NiO are in spinel and rock salt structures, respectively. Applying positive potential can transform rock salt structure into layered hydroxide and/or oxyhydroxide structures in alkaline solution, which may give better water oxidation activity than spinel structure.[7] For alcohol oxidation, there are limited reports on the influence of structure transformation and most reports focused on the comparison among Ni-doped Co_3O_4, cobalt oxides, and nickel oxides.[10,13,15] Note that for both small organic molecule oxidation reaction and water oxidation reaction, the catalytic mechanism involves the change of valence states of cations, during which the lower-state Ni and Co cations are firstly oxidized to the higher-state ones and then these higher-state cations oxidize the object.[2,7,8,10,14–16] Although there are some investigations on the composition effect on water oxidation reaction on Ni-Co oxides,[6,7,14] relevant reports on the composition effect on small organic molecule oxidation on Ni-Co oxides are rare. Our recent study has found that the performance of Ni-Co oxides toward methanol (MeOH) electrocatalytic oxidation varies with the Ni content and the best performance can be found at the Ni content of 46%.[17] To date, as the smallest alcohol molecule, methanol has been intensively investigated and reported with regarding to its oxidation reactions on noble metals, alloys, and oxides.[2,13,15,17] Similarly, the approach is extended to investigate the electrochemical oxidation of slightly bigger alcohols, such as C2 alcohols EG and EtOH. The research has been given on noble metals and their alloys.[18–21] However, the research on EG and EtOH oxidation on transition metal oxides are very limited.[22,23] Here, we present a first systematic investigation on the composition influence of Ni-Co oxides on their electrocatalytic activity toward EG and EtOH oxidation. We found that the activity of Ni-Co oxides toward EG and EtOH oxidation is composition dependent. The highest activity was found at 46% Ni. The effect of Ni and the influence of OH^- concentration on EG and EtOH oxidation were investigated as well. Nuclear magnetic resonance (NMR) analysis revealed that the oxidation of EG and EtOH was through the oxidative conversion of hydroxyl group to carboxyl group.

Experimental

Materials and characterizations.— The Ni-Co oxides were prepared by the electrodeposition of Ni-Co hydroxides on stainless steel mesh (SSM, 500 mesh, 1.0 cm × 1.0 cm) substrates followed by annealing in air.[17] The electrolyte consisted of x M $Ni(NO_3)_2$ and (0.1 – x) M $Co(NO_3)_2$. The value of x was set as 0, 0.03, 0.05, 0.07, 0.09 and 0.1. A Bio-Logic SP150 potentiostat was used for electrodeposition. A constant potential −0.85 V vs. saturated calomel electrode (SCE) was applied until the passing charge reached 0.6 C at room temperature. As for the pure $Ni(NO_3)_2$ electrolyte, the passing charge was controlled at 0.8 C in order to keep NiO mass loading similar to other samples. The crystal structure and morphology can be found in our previous report.[17] The three-electrode system was used to characterize the working electrodes of NCOs/SSM. Cyclic voltammetry (CV), differential pulse voltammetry (DPV), multi-step chronoamperometry (CA), and electrochemical impedance spectroscopy techniques (EIS) methods were employed to study the EG and EtOH oxidation reaction on NCOs. A Hg/HgO (1 M KOH, aqueous) electrode was used as the reference electrode and a Pt plate (~1.0 cm × 3.0 cm) was used as the counter electrode. The CV test was conducted from −0.1 ~ 0.6 V vs. Hg/HgO electrode at the scan rates of 2, 5, 10, 20, 40, and 80 mV s^{-1} in the absence and the presence of EtOH and EG, respectively. The CV curves at 2 mV s^{-1} were selected for fitting Tafel plots. The multi-step CA was conducted according to the following procedure. First, the working electrode was held at 0 V for 2 min. Then, it was held for 10 min at 0.48, 0.51, 0.54, 0.57, 0.60, 0.57, 0.54, 0.51, and 0.48 V, respectively. The DPV was carried on at 10 mV s^{-1} and with the pulse height 2.5 mV. EIS measurements were taken at bias potentials of 0.48, 0.51, 0.54, 0.57, and 0.60 V consecutively with 10 mV amplitude. The frequency ranged from 1 MHz to 10 mHz and the data were collected and processed from 100 kHz to 10 mHz. The products

[z]E-mail: xuzc@ntu.edu.sg

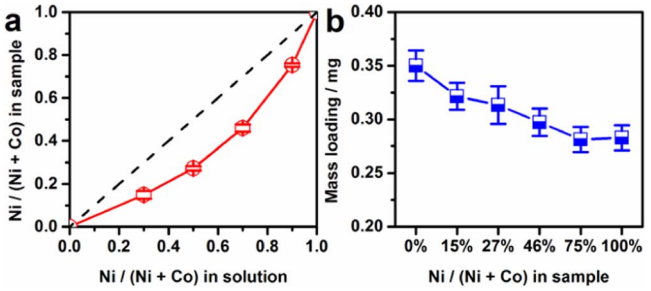

Figure 1. (a) The relationship between Ni / (Ni + Co) in samples and Ni / (Ni + Co) in precursor solutions; (b) the mass loadings of NCOs with different Ni / (Ni + Co) in samples.

of EG and EtOH oxidation were analyzed by a Bruker Avance 300 (200 MHz) NMR spectrometer.

Results and Discussion

NCO electrodes.— Fig. 1a shows the relationship between the composition of NCOs and the feeding ratio of precursor solutions. With the increase of the Ni salt concentration in the precursor solution, the ratio of Ni / (Ni + Co) in samples increased gradually from 0% to 15%, 27%, 46%, 75% and finally 100%. Here, the Ni content refers to the ratio of Ni / (Ni + Co) in as-synthesized NCOs. These samples were named as NCO-0, NCO-15, NCO-27, NCO-46, NCO-75, and NCO-100, referring to the NCOs with 0, 15, 27, 46, 75, and 100% Ni correspondingly. The mass of NCOs decreased with the increase of the Ni content (Fig. 1b). As for pure NiO, the passing charge was tuned to 0.8 C to maintain the similar mass loading to other Ni-Co oxides and pure Co_3O_4. The error bars in Fig. 1 were obtained based on three independent electrodeposition experiments. It can be seen that the variation of the composition and the mass of the NCO electrodes is small, indicating the high reproducibility of these electrodes.

CV measurements for EG and EtOH oxidation.— The two C2 alcohols, EtOH and EG, were investigated for the electrocatalytic performance of NCOs in 1.0 M KOH from −0.1 ∼ 0.6 V vs. Hg/HgO. Fig. 2a shows the CV curves of NCOs in 1.0 M KOH solution at 10 mV s^{-1}. More detailed information can be found in our previous report.[17] Figs. 2b and 2c shows the CV curves of EG and EtOH oxidation on NCOs in 1.0 M KOH with 0.5 M alcohol (EG or EtOH) at 10 mV s^{-1}, respectively. Fig. 2d shows the currents at 0.6 V from CV curves. It shows that as the Ni content increased, the EG and EtOH oxidation currents firstly increased and then decreased. The highest oxidation currents appeared when the Ni content is 46%. This trend is similar to what have been observed in MeOH oxidation.[17]

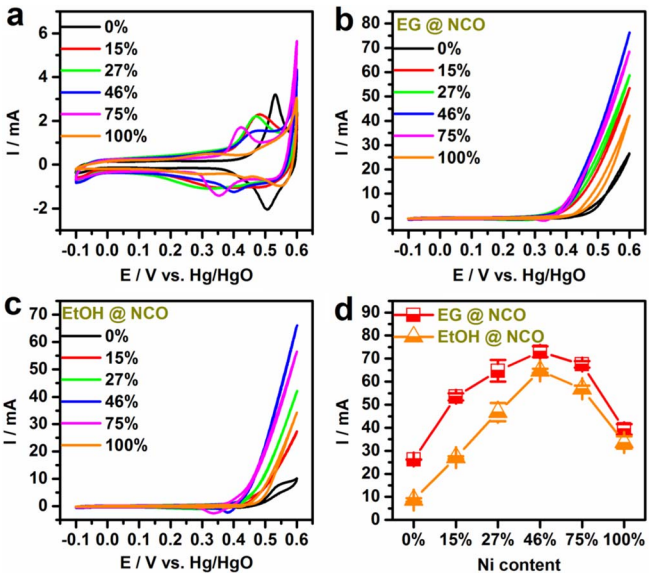

Figure 2. (a) CV curves of NCOs in 1.0 M KOH solution; CV curves of EG (b) and EtOH (c) oxidation on NCOs in 1.0 M KOH; (d) the currents at 0.60 V vs the Ni content.

The CV curves at 2 mV s^{-1} of EG and EtOH oxidation on NCOs were used to fit Tafel plots, which are shown in Fig. S2a and Fig. S2b. Fig. S2c shows the summary of Tafel slopes. In general, the Tafel slopes of EtOH oxidation were smaller than those of EG oxidation, which indicates that EtOH oxidation is faster than EG oxidation.

Multi-step CA measurements of EG and EtOH oxidation.— The multi-step chronoamperometry was used to further characterize EG and EtOH oxidation on NCOs. Fig. 3a shows the results of multi-step CA measurements of EG oxidation on NCOs. The EG oxidation currents firstly increased and then decreased as the potential was changed from 0.48 to 0.60 and then back to 0.48 V step by step. In Fig. 3a, the EG oxidation currents on NCOs (except for NiO) decayed within each potential step when the potential step was raised from 0.48 to 0.54 V. The current decay can be ascribed to the gradual adsorption and accumulation of oxidation intermediate products at different potential steps. When the potential steps was 0.60 V, the currents on NCOs with high Ni contents like NCO-46 and NCO-75 were more stable, while the currents on NCOs with low Ni contents like NCO-15 and NCO-27 still showed the decay. It suggests that the intermediate products probably could be fully oxidized on NCO-46 and NCO-75 at 0.6 V. As for those NCOs with low Ni contents like NCO-15 and NCO-27, the oxidation intermediate products could not be fully

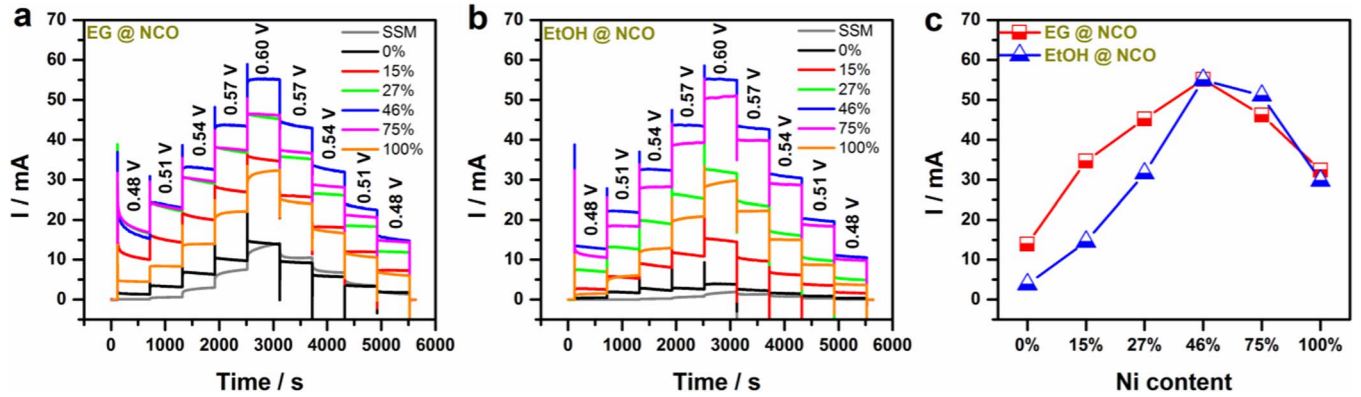

Figure 3. The multi-step CA curves of EG (a) and EtOH (b) oxidation on SSM and NCOs/SSM in 1.0 M KOH + 0.5 M alcohol (EG or EtOH) at the bias potential 0.48, 0.51, 0.54, 0.57, and 0.60 V vs. Hg/HgO; (c) the currents at the last second of the 0.60 V step.

oxidized at 0.60 V. It blocked the electrode surface and resulted in the current decay. When the potential steps changed from 0.60 back to 0.48 V step by step, all NCOs showed the current decay within 0.57, 0.54, 0.51 and 0.48 V steps, indicating the accumulation of intermediate products again on the electrode surface. It can be noticed that all the currents on NCOs at the potential step after 0.60 V was smaller than that at the same potential step before 0.60 V. It further indicates that the adsorbed intermediate products accumulated as the reaction progressed. As for pure NiO, the current did not show the decay when the potential changed from 0.48 to 0.60 V. When the potential steps were 0.57 and 0.60 V, the current increased gradually as the reaction progressed. It probably can be ascribed to the NiO activation. When the potential changed from 0.60 back to 0.48 V, the current showed obvious decay within each potential step. It indicates that more oxidation intermediate products were generated at the previous high potential step. Due to a stronger adsorption, they cannot be released quickly from the electrode surface and thus they began to block the surface. It is known that in the absence of convection, the diffusion limit can cause the decay of the current.[24] Here, the diffusion limit can be excluded by comparing EG oxidation on NiO and NCO-75. It can be seen in Fig. 3a that NCO-75 gave the bigger current than pure NiO within the same potential steps, implying more EG was consumed on NCO-75 than NiO. However, EG oxidation on NCO-75 did not show obvious current decay. It indicates that the diffusion of EG should be fast enough to supply the reaction need and thus it is not a factor that causes the current decay. Fig. 3b shows the results of multi-step CA measurements of EtOH oxidation on NCOs from 0.48 V to 0.60 V and then back to 0.48 V step by step. It exhibited a similar current change trend as observed in EG oxidation (Fig. 3a). In overall, the EtOH oxidation currents firstly increased and then decreased when the potential changed step by step from 0.48 to 0.60 and then back to 0.48 V. It is noted that the EtOH oxidation currents showed obvious current decay on NCO-0, NCO-15, and NCO-27 within each potential step. Meanwhile, the currents on NCO-0, NCO-15, NCO-27, and NCO-46 at each potential step after 0.60 V were smaller than those before 0.60 V at the same potential step. Fig. 3c summarizes the currents from last second in 0.6 V in Figs. 3a and 3b. It shows that the EG and EtOH oxidation currents firstly increased and then decreased. The biggest currents from EG and EtOH oxidation appeared at Ni 46%. Such a relationship between the composition and the oxidation current has been also observed in CV measurements.

EIS measurements for EG and EtOH oxidation.— EIS was used to further study EG and EtOH oxidation on NCOs. Fig. S6 and Fig. S7 shows the Nyquist plots and Bode Z plots of EG and EtOH oxidation on NCOs. In Fig. S6, the Nyquist plots of EG oxidation on NCO-15, NCO-27, and NCO-46 gave some data points below zero (Fig. S6d, g, j), which are often ascribed to the resistance-inductance series (shown in Fig. S8b). The inductive behaviour is due to the adsorption, re-generation, and re-adsorption of the active sites.[25,26] The Nyquist plot of EG oxidation on Co_3O_4 did not show obvious data points below zero (Fig. S6a). It is probably due to the adsorption of oxidation intermediate products on the surface of electrode and no new active site re-generated (Fig. S8a). Back to the multi-step CA curves on Co_3O_4 (Fig. 3a), it can be found that the current was small and decay obviously at the potential steps of 0.51, 0.54, and 0.57 V. This decay is ascribed to the facts that the active sites were occupied by EG oxidation intermediate products and no new active sites generated. As for the Nyquist plots of NCO-75, there were almost no data points below zero (Fig. S6m), which suggested that the charge transfer and intermediate product adsorption are more critical than the adsorption and re-generation of active sites. The Nyquist plots of EG oxidation on NiO show two distinct depressed semi-circles (Fig. S6p). As the bias potential increased, the diameters of these two semi-circles decreased. We assumed that these two depressed semi-circles represented two step reactions. The depressed semi-circles in low-frequency region can be ascribed to the reaction from EG to intermediate products along with intermediate product adsorption. The depressed semi-circles in the high-frequency region can be ascribed to the step from intermediate products to final products. In Fig. S6p, the oxidation rate of EG intermediate products absorbed on NiO was promoted as the potential increased and thus the diameter of the depressed semi-circles decreased. Meanwhile, the increase of potential promoted the reaction from intermediate products to final products, leading to the decrease of the diameter of the depressed semi-circles in the high-frequency region. It is noted that when the Ni content was higher than 46%, the data points below zero representing adsorption and re-generation of active sites disappeared (Fig. S6m and p) and data points on depressed semi-circles in low-frequency region representing intermediate product adsorption became distinct (Fig. S6p). Combining with the results from CV (Fig. 2d) and CA (Fig. 3c), the composition dependence of NCOs for EG oxidation can be suggested. When Ni content was lower than 46%, the EG oxidation increased with the increase of Ni content. It suggested that the increase of Ni content can facilitate the overall oxidation process through promoting the steps from EG to the intermediate products and from intermediate products to final products. However, probably the promotion on facilitating the step from intermediate products to final products is not significant. It leads to the accumulation of produced excessive intermediate products. As a result, more and more intermediate products accumulated on the electrode surface and thus the regeneration of active sites cannot be observed. Only at a Ni content of 46%, the two step reaction rates were balanced at the best ratio and thus the highest activity can be observed on NCO-46. Fig. S7 shows the EIS results of EtOH oxidation on NCOs. The EtOH oxidation on NCO-0 (Fig. S7a), NCO-15 (Fig. S7d), and NCO-27 (Fig. S7g) shows the obvious EtOH oxidation intermediate product adsorption. As for pure Co_3O_4, this strong adsorption led to the gradual increase of the diameter of the depressed semi-circles at 0.51, 0.54, and 0.57 V in Fig. S7a. It is probably because that increasing potential brought about more adsorbed intermediate products from EtOH oxidation so as to block the reaction. At 0.60 V, the smaller diameter of depressed semicircle means these EtOH were able to be oxidized (Fig. S7a). In Fig. S7d and g, it can be also found that even though the potential increased from 0.51 to 0.54, to 0.57 V, the diameter changed very little, indicating no change in impedance. It further implies that the intermediate product adsorption hindered the resistance decrease.

The impedance Z vs. the bias potential was summarized to compare EG and EtOH oxidation on NCOs (shown in Fig. 4). When the bias potential increased, all the impedance of EG and EtOH oxidation on NCOs decreased except for EtOH oxidation on Co_3O_4. In general, the impedance decrease is due to the promoted oxidation reaction with the increase of the bias potential. In Fig. 4b, the impedance of EtOH oxidation on Co_3O_4 did not show this general change. The impedance decreased from 0.48 to 0.51 V, and then increased from 0.51 to 0.57 V. Finally it decreased again from 0.57 to 0.60 V. Such an irregular change of the impedance of EtOH oxidation on Co_3O_4 may be ascribed to the accumulation of the intermediate products after 0.51 V. With the increase of potential, more intermediate products accumulated on the electrode surface. The reaction was gradually blocked until 0.6 V was applied, where the intermediate products could be fully oxidized, leaving a cleaned surface for more reactions. This has not

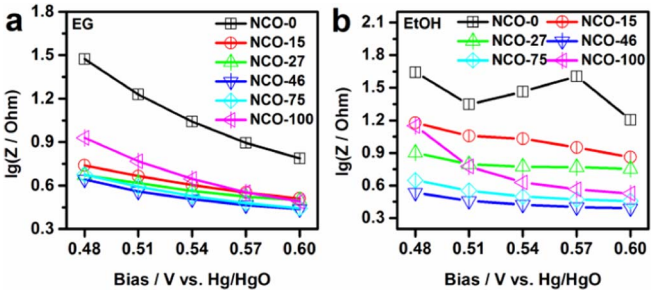

Figure 4. The impedance Z vs the bias potential for EG (a) and EtOH (b) oxidation on NCOs.

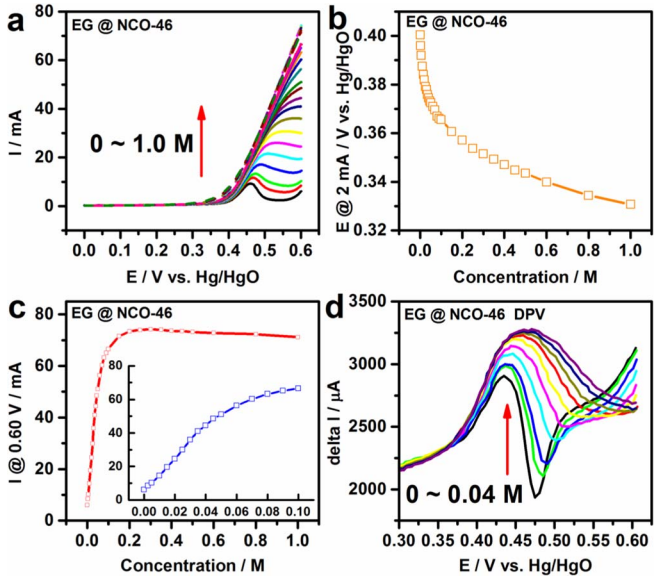

Figure 5. The EG oxidation on NCO-46 with different EG concentration: (a) LSV curves at 10 mV s^{-1}; (b) the potential at 2 mA vs. concentration; (c) the current at 0.60 V vs. concentration (the inset shows the close view on the concentration range of 0 ~ 0.1 M; (d) DPV curves at 10 mV s^{-1} and pulse height 2.5 mV.

been observed in EG oxidation on Co_3O_4 (Fig. 4a). It indicates that the intermediate products from EtOH oxidation may be more difficult to be oxidized as compared with those from EG oxidation. Such an assumption should be possible because EG has two hydroxyl groups at the two ends and it may reduce difficulties for electrode to oxidize the two hydroxyl groups at the same time. Only with the presence of Ni, the oxidation of the intermediate products of EtOH oxidation can be promoted and therefore NCOs did not exhibit such an impedance change trend as Co_3O_4 did. In addition, it may be noticed that with the increase of Ni content, the trend of the impedance change was opposite to the trend of the current change observed in CV and multi-step CA approaches (shown in Fig. 2d and Fig. 3c). EG and EtOH oxidation on NCO-46 shows the smallest impedance. It is consistent with the Ohm's law that the impedance is inversely proportional to the current at the fixed potentials.

EG and EtOH oxidation on NCO-46.— NCO-46 with the best performance was chosen to investigate the EG and EtOH concentration effect. Fig. 5a shows the LSV curves of EG oxidation on NCO-46 as the EG concentration was varied from 0 to 1.0 M. As the EG concentration increased, the currents increased. When the EG concentration was low, the oxidation peak of Co and Ni in NCO-46 in alkaline was remarkable. When the EG concentration was high, the curve ramped along the anodic sweeping direction. This phenomenon can be also found from DPV curves (Fig. 5d). The DPV peaks shifted to the higher potential region and became broader. The DPV currents increased with the increase of the concentration. Fig. 5b shows the relationship between the potential at the current of 2 mA and the EG concentration. It is observed that with the increase of EG concentration, the potential at 2 mA decreased. It indicates that increasing the EG concentration promoted the reaction rate. Fig. 5c summarizes the current at 0.60 V in Fig. 5a. In the concentration range of 0 ~ 0.04 M, the current change increased approximately linearly with the EG concentration increase. Between 0.04 and 0.2 M, the current kept increasing, however, the increase was slow. As the EG concentration was close to 0.2 M, the current stopped increasing and reached a saturation state. When the EG concentration was higher than 0.2 M, the currents decreased slightly with the further increase of concentration. Comparing Fig. 5b and Fig. 5c, it can be noted that in Fig. 5b the potential at 2 mA decreased gradually with the increase of EG concentration, while in Fig. 5c the current firstly increased and then slightly decreased with the increase of EG concentration. Here, the potential in Fig. 5b was recorded at relatively small current 2 mA and the current in Fig. 5c was recorded at relatively high potential 0.60 V. As for the relationship between current and EG concentration in Fig. 5c, it can be explained as follow. When the EG concentration was lower than 0.2 M, the oxidation rate determined by the reactant concentration and increasing EG promoted the oxidation reaction rate. When the EG concentration was higher than 0.2 M, the ability of OH^- supply to the electrode surface cannot meet the EG oxidation rate. Thus, the EG oxidation reaction cannot be promoted further. In addition, a slight decrease of the current can be found as the EG concentration increased further. It is probably due to the increase of solution viscosity. With the increase of EG concentration in solution, the viscosity (η) of solution increased.[27] The increase of solution viscosity led to the decrease of EG diffusion coefficient (D) according to the equation,

$$D = RT/6N_A\pi\eta a$$

where N_A is Avogadro's number, R is gas constant, T is thermodynamic temperature, and a is hydrodynamic radius.[28,29] The concentration effect on EtOH oxidation is shown in Fig. S9. EtOH oxidation currents reached saturation state at higher concentration (~1.25 M) as compared to EG oxidation (~0.2 M). At the relatively high concentration, EtOH oxidation showed a higher current than EG oxidation. For example, when the concentration was 1.0 M at 0.60 V, EtOH oxidation showed the current of ~80 mA, while EG oxidation gave the current of ~71 mA. It is probably due to the lower viscosity of EtOH and thus better EtOH diffusion.

The influence of KOH concentration on EG oxidation.— The NCO-46 electrode was used to investigate the influence of KOH concentration on EG oxidation. Five different concentrations were chosen: 0.01, 0.1, 1.0, 3.0, and 5.0 M. The EG concentration was kept at 0.5 M. Fig. S10a shows the CV curves with the applied potentials vs. Hg/HgO and Fig. S10b shows the CV curves with the applied potentials converted to the potentials vs. reversible hydrogen electrode (RHE). CV curves in Fig. S10a and Fig. S10b show that with the increase of KOH concentration, the EG oxidation current became bigger. It suggested that the high concentration of KOH facilitated EG oxidation. When the KOH concentration was lower than 1.0 M, the EG oxidation current was very small. The Nyquist plots of EG oxidation on NCO-46 in 0.1, 1.0, 3.0, and 5.0 M are shown in Fig. S10c, d, e and f. In Fig. S10c, when the KOH concentration was 0.1 M, the Nyquist plots showed the high impedance reflected by the big diameter of the depressed semi-circles. Meanwhile, when the bias potential increased, it is observed that the low-frequency region displayed diffusion phenomena from 0.54 V. From the previous analysis on EG concentration effect in Fig. 5b, 0.5 M EG was enough to supply the EG oxidation reaction in 1.0 M KOH. EG oxidation had a faster reaction rate in 1.0 M KOH than in 0.1 M KOH (it can be seen in Fig. S10a and b). Since EG supply was enough, these diffusion phenomena in low frequency region shown in Fig. S10c should represent the OH^- diffusion limit on EG oxidation. In Fig. S10c, it can be observed that the Nyquist plots were almost the same when the bias potential was 0.63 V and 0.66 V. It suggests that when the bias potential was higher than 0.63 V, EG oxidation was not limited by the bias potential any more, but the OH^- supply. The low current and big impedance also can be ascribed to insufficient OH^- supply. Due to the limited OH^- supply, the oxidation of EG was hindered. The prevailing mechanism of alcohol oxidation on NCO is that the low valence Ni and Co cations were oxidized to the high valence state ones. And then alcohol is oxidized by the high valence state Ni and Co cations.[17] However, the low valence Ni and Co cations were more difficult to be oxidized to the high valence state of Ni and Co in the lower concentration of KOH solution as seen in Fig. S11. When the KOH concentration was higher than 1.0 M in Fig. S10d, e and f, the diffusion phenomena were not observed in the low-frequency region of the Nyquist plots. However, the adsorption and re-generation phenomena of active sites were more obvious, which can be seen from more data points located below zero. Meanwhile,

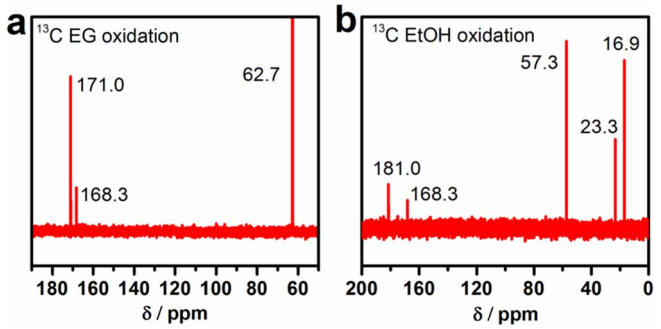

Figure 6. The ^{13}C NMR spectra of the electrolyte solutions after 12 hours of EG (a) and EtOH (b) oxidation.

the diameters of these depressed semi-circles decreased with the increase of KOH concentration and the increase of bias potential. It suggested that the high concentration of OH^- facilitated the oxidation reaction and led to more adsorption and re-generation of active sites. In addition, the influence of KOH concentrations was reflected in the resistance in solution, which can be seen from the Nyquist plots (the intersection point with horizontal axis in Fig. S10c-f). This resistance observed at high frequency regions includes the solution resistance and the resistance caused by EG intermediate product accumulation on the electrode surface. The higher the KOH concentration is, the smaller the resistance is. As for EG oxidation on NCO-46 in 0.01 M KOH solution, the resistance in solution was quite big and it became bigger and bigger with the increase of the bias potential (shown in Fig. S12a). It suggests that the insufficient supply of OH^- suppressed the complete oxidation of EG and the intermediate products were gradually accumulated on the electrode surface with the increase of the potential. It can be also seen in the CV measurements right after the EIS measurements (Fig. S12b). The currents after EIS measurements were apparently smaller than that before EIS measurements, suggesting that the EG oxidation intermediate products adsorbed on the electrode surface led to the current drop after the polarization. It should be noted that the concentration of KOH also influenced the resistance of the electrolyte solution. In particular, a very low concentration may give a significant iR drop. Fig. S13 shows the EG oxidation LSV curves recorded in different concentrations of KOH solution. The potential was corrected by iR drop. It is obvious that the higher concentration of KOH solution facilitated the EG oxidation. For example, the oxidation can be promoted in 3 and 5 M KOH as compared to those performed in 1, 0.1, and 0.01 M KOH. This indicates that OH^- was involved in the reaction as a reactant. In addition, the CA curves of the EG and EtOH oxidation on NCOs are shown in Fig. S14-S17. It can be seen that NCO-46 exhibited the higher stability.

NMR analysis on EG and EtOH oxidation.— The products of the EG and EtOH oxidation on NCO-46 were measured by NMR. Fig. 6 shows the NMR spectra of the electrolyte solutions after EtOH and EG oxidation for 12 hours at 0.60 V. In Fig. 6a, the peak at 62.7 ppm can be assigned to EG[30] and the peak at 171.0 ppm can be assigned to oxalic acid (COOH-COOH). In Fig. 6b, the resonance peaks in 16.9 and 57.3 ppm can be assigned to ethanol[30] and the peaks in 23.3 and 181.0 ppm can be assigned to acetic acid (CH_3-COOH).[30] The peak in 168.3 ppm in Figs. 6a and 6b are assigned to carbonate (CO_3^{2-}),[31] which is due to the adsorption of CO_2 in the electrolyte solution. The theoretical study has pointed out that the formation CO_2 from C-C bond cleavage through C2 alcohol oxidation is difficult.[32] Several studies have also shown that there is no cleavage of C-C bond observed in the ethanol oxidation on transition metals in alkaline and the cleavage of C-C bond was only found on noble metal catalysts.[33,34] Thus, the small peak at 168 ppm should be ascribed to the carbonate from the adsorption of CO_2. The NMR result indicates that the major products of EG and EtOH oxidation were oxalic acid (COOH-COOH) and acetic acid (CH_3-COOH), respectively. We believe that the intermediate products of EG and EtOH oxidation should be some aldehyde compounds such as glyoxal (CHO-CHO), acetaldehyde (CH_3-CHO), etc. However, we didn't found these intermediates in the electrolyte solution. It indicates that these aldehyde intermediates only exist on the electrode surface during the oxidation.

Given the above analysis on the influence of KOH concentrations as well as the NMR result, the EG and EtOH oxidation can be expressed as follows:

EG oxidation to oxalic acid:

$$CH_2OH\text{-}CH_2OH + 4OH^- \rightarrow CHO\text{-}CHO + 4H_2O + 4e^-$$

$$CHO\text{-}CHO + 6OH^- \rightarrow {}^-OOC\text{-}COO^- + 4H_2O + 4e^-$$

EtOH oxidation to acetic acid:

$$CH_3\text{-}CH_2OH + 2OH^- \rightarrow CH_3\text{-}CHO + 2H_2O + 2e^-$$

$$CH_3\text{-}CHO + 3OH^- \rightarrow CH_3\text{-}COO^- + 2H_2O + 2e^-$$

It can be seen that increasing OH^- concentration will facilitate the oxidative conversion from hydroxyl group to carboxyl group. It should be noted that our EtOH oxidation product is different from that observed in EtOH biofuel cells and sensors catalysed by enzyme quino-hemoprotein-alcohol dehydrogenase (QH-ADH),[35–38] where the EtOH is oxidized to acetaldehyde only. The oxidation is catalysed by the enzyme QH-ADH and the reaction is described as follow:

$$CH_3\text{-}CH_2OH \rightarrow CH_3\text{-}CHO + 2H^+ + 2e^-$$

The reaction provides two protons and two electrons through the oxidation of hydroxyl group to aldehyde group. Such an enzyme catalysed reaction was found pH dependent as well. The highest reaction efficiency was found at the pH range of 5 ∼ 6 by Ramanavicius et al.[35,36] However, the enzymatic catalyst-based fuel cells and sensors are not stable, especially operated for a long period because of the fragile nature of the enzymes and limited immobilization techniques[36,39] Thus, the development of non-enzymatic electrocatalysts is desired in this field. The Ni-Co oxide catalysts reported here may be potential for similar biofuel cell and sensor systems. The advantages may include better stability and higher oxidation degree of hydroxyl group to carboxyl group. However, it should be noted that these catalysts work in alkaline and the higher pH facilitates the reaction. Therefore, their application should be limited in those biofuel cells and sensors in alkaline environments.

The reaction charge (Q) of EG and EtOH.— In this section, the oxidation degrees of hydroxyl groups of EG and EtOH are further compared based on the above NMR analysis, in which it was found that EG and EtOH oxidation process is the conversion from hydroxyl group to carboxyle group. Both EG and EtOH are C2 alchohol. The EtOH molecule has one hydroxyl group, while the EG molecule has two. Here the reaction charge, Q, was used to describe and compare the oxidation degree of hydroxyl groups. Q(EG) and Q(EtOH) on NCO-46 can be calculated by integrating the I-t curves at different potentials in Figs. 3a and 3b. Fig. 7a shows that Q(EG) and Q(EtOH) were almost the same at the relatively high potential like 0.54, 0.57, and 0.60 V, while Q(EG) was higher than Q(EtOH) at the relatively low potential like 0.48 and 0.51 V. Fig. 7b shows the values of Q(EG)/Q(EtOH). At relatively low potentials like 0.48 and 0.51 V, the value of Q(EG)/Q(EtOH) is between 1 and 2. At relatively high potentials like 0.54, 0.57, and 0.60 V, Q(EG)/Q(EtOH) is nearly 1. Two possibilities can be proposed to explain the phenomenon that Q(EG)/Q(EtOH) had different ratio values at high and low potentials. One is the influence of EG and EtOH diffusion. Here, viscosity (η), diffusion coefficient (D), and Schmidt number (Sc) can be used to compare to the difference between EG and EtOH fluid mechanics. From Table S1, EG has a bigger η, smaller D, and bigger Sc, than EtOH in water.[40] Thus, EG is more difficult to diffuse onto the working electrode than EtOH. When EG and EtOH are consumed fast on the electrode surface at a high potential, EtOH has a higher supply

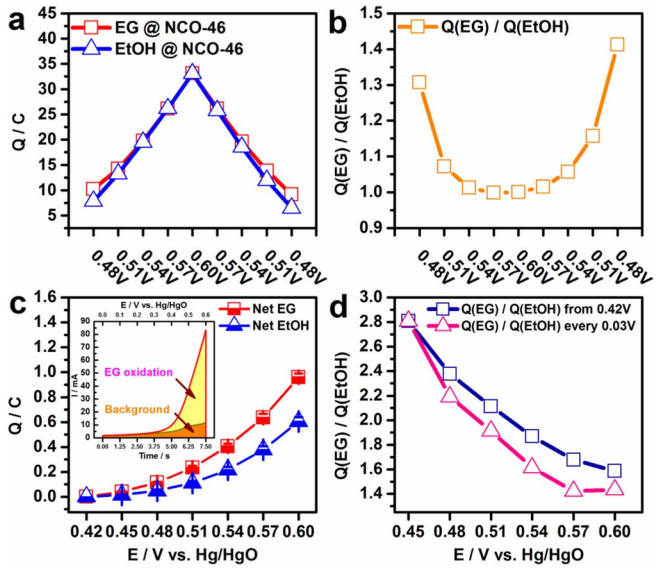

Figure 7. (a) The reaction charge Q obtained from the multi-step CA approach (Figs. 3a and 3b) at different potential steps; (b) the ratio of Q(EG)/Q(EtOH) from Fig. 7a; (c) the net reaction charges of EtOH and EG oxidation from 0.42 V to each specific potential. The inset shows the LSV curves of NCO-46 in the absence and the presence of EG at 80 mV s^{-1}; (d) the ratio of the net EG reaction charge to the EtOH reaction charge from 0.42 V to each specific potential (hollow cubic) and the ratio of the net EG reaction charge to the EtOH reaction charge within every 0.03 V step from 0.42 V (hollow triangle).

rate than EG. It leads to more EtOH oxidized and the similar reaction charge at high potentials. At low potentials, there is no big difference between the difusion rate of EG and EtOH and therefore the supply of two alchohls is enough for the reaction need. Thus, the charge involved in their oxidation reactions is determined more by the numbers of hydroxyl groups. Another possibility is that not both of hydroxyl groups in EG are oxidized at the same time. To further analyze these two possibilities, the anodic scans in CV curves (Fig. S1) at the higher scan rate of 80 mV s^{-1} were compared with multi-step CA curves. The fast test of CV at high scan rates can avoid the influence of the consumption of EG and EtOH. The reaction charge (Q) can be obtained by the equation

$$\mathbf{Q} = \frac{1}{v}\int i\,du,$$

Where i and u are the current and the potential recorded in anodic scans in CV curves, respectively, and v is the scan rate of CV. Fig. 7c shows that the integrated net Q (Q(EG) – Q(background)) from 0.42 V to the specitific potential. With the potential increasepotential, the Q increased. Q(EG) was bigger than Q(EtOH). Fig. 7d shows that the two kinds of Q(EG)/Q(EtOH). One is the value from 0.42 V to the specific potential and the other one is the value at every 0.03 V step, like the steps of 0.42 ∼ 0.45 V and 0.45 ∼ 0.48 V. It can be found that generally the value of Q(EG)/Q(EtOH) is bigger than 1. At relatively low potentials, the value of Q(EG)/Q(EtOH) is bigger than 2. This is different from the values observed in multi-step CA curves. It further indicates that the charge associated in the EG and EtOH oxidation is indeed determined by the supply of EG and EtOH through diffusion. The different diffusion properties of EG and EtOH results in the difference in the reaction charges. At the relatively low potential, the influence of the comsumption of reactants was little and thus the charge assocaited with the EG oxidation and the EtOH oxidation was determined by the number of hydroxyl groups on each molecule.

Conclusions

In summary, a detailed investigation has been conducted on the electro-oxidation of EG and EtOH on Ni-Co oxides with various compositions. It was found that Ni-Co oxide with 46% Ni (NCO-46) showed the best oxidation performance for both EG and EtOH. EIS study reveals that the more Ni component in the oxide may facilitate the oxidation reaction. The NCOs with low Ni contents exhibited low reaction rates and it is probably due to the strong adsorption of oxidation intermediate products, which blocked the reaction sites. The high concentration of KOH can facilitate the oxidation reaction because OH^- is a reactant in EG and EtOH oxidation reactions. The complimentary study by NMR shows that the oxidation of EtOH and EG is due to a chemical conversion from hydroxyl group to carboxyl group.

Acknowledgments

This work was supported by the MOE Tier 1 Grants (RG131/14 and RG13/13) of Singapore, and the Singapore National Research Foundation under its Campus for Research Excellence And Technological Enterprise (CREATE) programme. Authors thank the Facility for Analysis, Characterisation, Testing and Simulation (FACTS) in Nanyang Technological University for materials characterizations.

References

1. H. Wang, J. Ye, Y. Liu, Y. Li, and Y. Qin, *Catal. Today*, **129**, 305 (2007).
2. R. Ding, L. Qi, M. Jia, and H. Wang, *Catal. Sci. Technol.*, **3**, 3207 (2013).
3. H. Shi and G. Zhao, *J. Phys. Chem. C*, **118**, 25939 (2014).
4. M. U. A. Prathap, B. Satpati, and R. Srivastava, *Electrochim. Acta*, **130**, 368 (2014).
5. T. H. Wesley, R. Marcel, A. S. Kelsey, Alexis Grimaud, S. Jin, and S.-H. Yang, *Energy Environ. Sci.*, **8**, 1404 (2015).
6. G. Wu, N. Li, D.-R. Zhou, K. Mitsuo, and B.-Q. Xu, *J. Solid State Electrochem.*, **177**, 3682 (2004).
7. L. Trotochaud, J. K. Ranney, K. N. Williams, and S. W. Boettcher, *J. Am. Chem. Soc.*, **134**, 17253 (2012).
8. R. Ding, L. Qi, M. Jia, and H. Wang, *Nanoscale*, **6**, 1369 (2014).
9. C. Zhang, L. Qian, K. Z. Zhang, S. Y. Yuan, J. Xiao, and S. Wang, *J. Mater. Chem. A*, **3**, 10519 (2015).
10. L. Gu, L. Qian, Y. Lei, Y. Wang, J. Li, H. Yuan, and D. Xiao, *J. Power Sources*, **261**, 317 (2014).
11. J. B. Wu, Z. G. Li, X. H. Huang, and Y. Lin, *J. Power Sources*, **224**, 1 (2013).
12. W. Wang, Y. Yang, Y. Liu, Z. Zhang, W. Dong, and Z. Lei, *J. Power Sources*, **273**, 631 (2015).
13. L. Qian, L. Gu, L. Yang, H. Yuan, and D. Xiao, *Nanoscale*, **5**, 7388 (2013).
14. Y. Li, P. Hasin, and Y. Wu, *Adv. Mater*, **22**, 1926 (2010).
15. M. U. Anu Prathap and R. Srivastava, *Nano Energy*, **2**, 1046 (2013).
16. M. Gao, W. Sheng, Z. Zhuang, Q. Fang, S. Gu, J. Jiang, and Y. Yan, *J. Am. Chem. Soc.*, **136**, 7077 (2014).
17. S. Sun and Z. J. Xu, *Electrochim. Acta*, **165**, 56 (2015).
18. S. Cherevko, N. Kulyk, and C. H. Chung, *Nanoscale*, **4**, 103 (2012).
19. J.-N. Zheng, J.-J. Lv, S.-S. Li, M.-W. Xue, A.-J. Wang, and J.-J. Feng, *J. Mater. Chem. A*, **2**, 3445 (2014).
20. Y. Kim, H. Kim, and W. B. Kim, *Electrochem. Commun.*, **46**, 36 (2014).
21. J.-N. Zheng, L.-L. He, F.-Y. Chen, A.-J. W. Wang, M.-W. Xue, and J.-J. Feng, *J. Mater. Chem. A*, **2**, 12899 (2014).
22. M. Shamsipur, M. Najafi, and M.-R. Milani Hosseini, *J. Appl. Electrochem.*, **43**, 1027 (2013).
23. P. Cox and D. Pletcher, *J. Appl. Electrochem.*, **20**, 549 (1990).
24. A. J. Bard and L. R. Faulkner, *Electrochemical methods: fundamentals and applications*, p. 35, John Wiley & Sons, Inc. (2001).
25. I. Danaee, M. Jafarian, F. Forouzandeh, F. Gobal, and M. Mahjani, *Int. J. Hydrogen Energy*, **34**, 859 (2009).
26. F. Seland, R. Tunold, and D. A. Harrington, *Electrochim. Acta*, **51**, 3827 (2006).
27. F. S. Jerome, J. T. Tseng, and L. T. Fan, *J. Chem. Eng. Data*, **13**, 496 (1968).
28. G. K. Batchelor, *J. Fluid Mech.*, **74**, 1 (1975).
29. D. J. Scott, S. E. Harding, and D. J. Winzor, *Analyst*, **139**, 6242 (2014).
30. H. E. Gottlieb, V. Kotlyar, and A. Nudelman, *J. Org. Chem.*, **62**, 7512 (1997).
31. S. Moret, P. J. Dyson, and G. Laurenczy, *Dalton Trans.*, **42**, 4353 (2013).
32. H. F Wang and Z. P. Liu, *J. Am. Chem. Soc.*, **130**, 10996 (2008).
33. C. Xu, Y. Hu, J. Rong, S. P. Jiang, and Y. Liu, *Electrochem. Commun.*, **9**, 2009 (2007).
34. J. Liu, J. Ye, C. Xu, S. P. Jiang, and Y. Tong, *Electrochem. Commun.*, **9**, 2334 (2007).
35. A. Ramanavicius, A. Kausaite, and A. Ramanaviciene, *Biosens. Bioelectron.*, **20**, 1962 (2005).
36. A. Ramanavicius, A. Kausaite, and A. Ramanaviciene, *Biosens. Bioelectron.*, **24**, 761 (2008).
37. A. Ramanavicius, A. Kausaite, and A. Ramanaviciene, *Sens. Actuators. B*, **113**, 435 (2006).
38. M. Niculescu, T. Erichsen, V. Sukharev, Z. Kerenyi, E. Csöregi, and W. Schuhmann, *Anal. Chim. Acta*, **463**, 39 (2002).
39. V. Oncescu and D. Erickson, *Sci. Rep.*, **3**, 1226 (2013).
40. D. R. Lide, *Handbook of Chemistry and Physics*, p. 6–181, CRC Press LLC (2002).